IEEE Access
Multidisciplinary ⋮ Rapid Review ⋮ Open Access Journal

Received June 30, 2019, accepted July 22, 2019, date of publication August 5, 2019, date of current version September 6, 2019.

Digital Object Identifier 10.1109/ACCESS.2019.2933235

Long Range Correlation in Vegetation Over West Africa From 1982 to 2011

TERTSEA IGBAWUA[1,3], JIAHUA ZHANG[1,2], FENGMEI YAO[2], AND SHAHZAD ALI[1]

[1]Remote Sensing Information and Digital Earth Center, College of Computer Science and Technology, Qingdao University, Qingdao, China
[2]College of Earth and Planetary Sciences, University of Chinese Academy of Sciences, Beijing, China
[3]Department of Physics, Federal University of Agriculture, Makurdi, Nigeria

Corresponding authors: Jiahua Zhang (zhangjh@radi.ac.cn) and Fengmei Yao (yaofm@ucas.ac.cn)

This work was supported in part by the National Key Research and Development Program of China under Grant 2016YFD0300110 and Grant 2016YFD0300101, in part by the China Postdoctoral Science Foundation under Grant 2019M652310, in part by the Key Basic Research Project of the Shandong Natural Science Foundation of China under Grant ZR2017ZB0422, in part by the Taishan Scholar Project of Shandong Province, and in part by the Qingdao's Postdoctoral Funded Project.

ABSTRACT Satellite-derived Normalized Difference Vegetation index (NDVI) data records offer important sources for long term correlation modelling over West Africa. In this study, we assessed long range correlations in half monthly NDVI records over West Africa from 1982 to 2011 using GIMMS NDVI. In our analysis, we assessed (a) the annual and seasonal trends obtained using Ordinary Linear Regression, (b) the detrended lag-1-autocorrelation $C(1)$, (c) the Detrended Fluctuation Analysis (DFA) scaling Hurst exponent h and (d) the Multifractal (MF) characteristics of NDVI. Results show that there exist some patterns or trends in the records that persist over time. The value of $C(1)$ for NDVI was obtained as 0.989 is significant at 95% confidence interval. Consequently, the scaling h values of the Hurst DFA showed that about 37.4, 20.5, 41.7 and 0.5% of the vegetated areas are anti-correlated ($h < 0.5$), un-correlated ($h = 0.5$), correlated ($0.5 < h < 1$) and uncorrelated random walk ($h = 1$), respectively. The trend analysis from Ordinary Least square Regression (OLR) shows that about 54.3, 0.1 and 45.6% of the vegetated areas are positively, uncorrelated and negatively correlated, respectively. Our findings revealed that the DFA method performed better than OLR and the findings could be useful in identifying areas with improved and degraded vegetation, which cannot be properly captured by the OLR method. Accordingly, the comparison of the MF-DFA results of original data to those of shuffled and surrogate series indicated that the multifractal nature of considered time-series is both from PDF and long-range correlations but arguably, MF due to long range correlation dominates over West Africa. The research is therefore helpful in the formulating crop and environmental management policies that may be used to improve ecosystem management using a long term plan (inter-annual) or short term (inter-seasonal) planning.

INDEX TERMS Long range correlation, multifractality, NOAA AVHRR, NDVI, ecological zones, West Africa.

I. INTRODUCTION

The vegetation of West Africa fluctuates rapidly both at spatial and temporal scales and the rate of fluctuation depends on the level of vegetation degradation and/or replacement [1], [2]. A lot of environmental factors are responsible for long-term vegetation degradation over the region, including naturally occurring processes [3] and human activities [4]–[11]. The naturally occurring processes could be erosion, drought, floods, population pressure, increased urbanization, and climatic change. Drought is a perennial feature of the West African Sahel, with devastating impacts on vegetation, soil and animal husbandry [4]. Vegetation has a good coupling with climate over the region [12], [13] and researches have shown that the depleted vegetation surface and rapid evaporation of moisture from the surface may have provided a positive feedback [14] that raises and sustains the droughts conditions [15]. The large fluctuations in vegetation trend in which there exist some multiplicity of control mechanism; possess scale invariant attributes defined by long range power law signal. Further, the values of vegetation in specific areas may exhibit autocorrelation (ACF) compared to the

The associate editor coordinating the review of this article and approving it for publication was Weipeng Jing.

values at regional scale. And the vegetation recovery rate in a specific location (say pixel level) is different compared to the average over the whole region of West Africa. The formal may not often be correlated while the later may be positively correlated. It is evident that the seasonal changes, inter-annual and directional fluctuations around the slope line are the critical variables in vegetation change monitoring, specifically in global and regional vegetation surface change [16]. Several methods are employed in the study of vegetation conditions [17] include (1) statistical techniques such as correlation, Principal Component Analysis (PCA) [18], curvefitting analysis [19]–[22] and fractal analysis [23]–[25]; (2) spectral frequency techniques such as spectral unmixing [26], [27], spectral mixture analysis [28], wavelets and spectral transform analysis [29], [30], and (3) Neural networks [31]. Of all the statistical methods, the most frequently used one is the Ordinary Least Square Regression (OLR) model, which is used in Trend analysis. The OLR is a robust and quick method but the major drawbacks are that, it is sensitive to data outliers and appears to exhibit symmetry around the maximum or minimum data values. Thus, it is cannot be used to properly assess vegetation expansion or degradation for areas with high spatial and temporal vegetation fluctuation.

In recent decades, the introduction of time scaling techniques in the characterization of long-range correlation of time series have attracted considerable attention and turned into a busy field of research, compared to short-range methods such as the Markov process [32]–[34] and auto regressive models [35], [36]. In long range correlations (persistence), the lag-1 detrended $ACF(C(1))$ and the scaling exponent called Hurst (h) are the basic variables [37]–[39]. Markovian processes are characterized with an exponential decay of their dwell times whereas non-Markovian processes are not [40]. Generally, Long-range correlations are likened to many chaotic systems [41], for which different methods and models in the Geoscience field have been developed [17], [40], [42], [43]. Short-range correlations are characterized by a decay such that the detrended $lag - s$ ACF is bounded by an exponential decay given as $C(s) \propto e^{-s/s_o}$ [21], [37], [38], [44] while long-range correlated time series are defined by power-law decay given as $C(s) \propto s^{-\gamma}$ [33], [37], [39], [40], [45]. The correlation exponent γ is computed by applying scaling laws where the Hurst exponent $H \approx \alpha = 1 - \gamma/2$ is obtained, and for $H > 0.5$ the system is considered long term correlated, $H = 0.5$ it is white noise, $H < 0.5$ it is long term anti-correlated while $H > 1$ it is a non-stationary local mean [40], [46]–[49]. Accordingly, this power-law decay of values can best be applied using the concept of self-similarity (self-affinity) [39] Self-affine/similar systems are also called fractals [50]–[52]. The concept was introduced by Mandelbrot and has been broadly applied in different disciplines [53]. Fractal dimension is directly linked to the strength of long-range correlations [17], [43]. and this relationship affects the suitability of arithmetic selected for any analysis. In a self-affine time series, the strength of the variations at a given frequency is given as a power-law function of that frequency and the scaling h exponent characterizes the type of self-affinity [39], [54], [55]. There are several methods that are developed to analyze self-similarity in the time series [56]. They include: Autocorrelation Function (ACF) , Spectral analysis, Hurst's Rescaled-Range analysis (R/S) and Fluctuation analysis [57], [58]. Fractals can be classified into two categories [39]: mono-fractals and multifractals. Mono-fractals are those, that are characterize with a single scaling exponent while multifractals are those that are defined with a large number of scaling exponents that are required for a detailed characterization of the scaling behavior of series [39], [56], [59], [60]. And so methods such as ACF, (R/S), and DFA are mono-fractal while MF-DFA is multifractal [37], [41], [42], [61]. ACF and R/S are strongly affected by length of times series while DFA is much free of size effects [33]. Multi-fractality could be as a result broad probability distribution density function (PDF) [57] and long range correlations (due to small and large fluctuations) [56]. Multifractality due to long range correlations can be removed by shuffling while the one due to PDF cannot be removed by time series shuffling [39].

In the last decade, long-range persistence and fractal scaling behaviors has been shown to be a part of many geophysical records [62], [63] including vegetation [39]. Analysis of the behavior of vegetation is less common compared to other fields of research especially over West Africa. The few examples used in studying fractals in vegetation are mono-fractal, and so the complexities involved in the formation of vegetation will not be exhaustively revealed. Also, the approaches did not incorporate long range correlation in time series of vegetation data. In one example, Song *et al.* (2006) [64] applied a box counting method to the vegetation distribution data collected from the vegetation map of the Xigaze region and results showed the power law of the box-counting dimension D_B across a range of scales (5-160 km) affirmed the fractal patterns for most vegetation formations, while the fluctuations of the scale-specific dimensions of the different batches indicated limitations of fractal consistency. In another example, the spatial scale-dependent variations in Mu Us sandy land in semi-arid area of Northwestern China were studied by Fu *et al.* (2013) [65]. The data sets were analyzed combining geostatistics and fractal geometry, and results showed that large fractal dimensions (>1.70) commonly found in the vegetation suggested dominance of small-scale variations. The switch in fractal dimensions was detected, indicating scale-dependent variation of vegetation as well as its hierarchical arrangement Jiapaer *et al.* (2015) [24] used the scaling Hurst exponent h to study the vegetation dynamics and responses to recent climate change in Xinjiang of China using leaf area index (LAI) as an indicator using a regression technique and Hurst exponent scaling method, and results revealed that the vegetation trend was consistent with a sustainable area of 51.18%, unsustainable area of 4.04% and stable and non-vegetated area ratio of 44.78%. Zhao *et al.* (2006) [66] studied on a fractal method of

estimating soil structure changes under different vegetation types on Ziwuling Mountains of the Loess plateau, China and the results suggested that collective fractal dimension is more efficient in outlining soil structure and function compared with particle fractal dimension. Guo *et al.* (2013) [67] studied long range correlation in vegetation over the greater Khingan Mountains using DFA method and results indicated that NDVI have self-similar properties. Guo *et al.* (2015) [68] evaluated the temporal scaling behavior of NDVI over China using DFA method and the analysis suggested that the NDVI time series displays strong long-range correlation throughout most of China with regional variability in the Hurst exponent h.

Previous researches on persistence in vegetation have focused on (1) the trends of vegetation indices, (2) fractal geometry and scaling properties of vegetation, and (3) relationships between them, limited efforts have been made to study the existence of multi-fractality in vegetation. In West Africa, it is to our knowledge that, no research on persistence and long range correction is yet to be done. In general, changes caused by climate and human activities, separately or jointly, sum up to vegetation changes on global and regional scales. Thus, it is vital to understand the persistence in NDVI data records which are obviously nonstationary, using some improved methods of time series analysis. Ordinarily, the OLR slope which has been utilized in assessing the areas with vegetation expansion and degradation may not properly reveal the exact nature of the vegetation changes, especially in areas with mixed land cover types and sparse vegetation. Thus, it is hoped that the application of fractal (self-similar) methodology to vegetation time series will reveal some important details about the vegetation changes over West Africa especially the Sahel region. There has been no comprehensive theory that describes the source of long term persistence in vegetation data sets over West Africa. However, studies have shown that climate variables like sea surface temperature (SST), temperature, precipitation, wind speed exhibit long range correlation and are persistent [38]. And since, researches over the region have proved a strong ocean-vegetation coupling [69]; it is therefore important to also know if vegetation data sets over West Africa are persistent and long range correlated.

The primary objectives of this research are to investigate: (1) the strength, presence/absence of long term correlations in NDVI over West Africa from 1982 to 2011, (2) the intriguing statistical properties and multifractal characteristics of the series and (3) if the long term correlations (if at all they exist) are due to PDF or long range correlations in NDVI. Our investigations are based on monofractal and multifractal analysis. We apply the detrended lag-1 ACF to assess the short range correlation and to also obtain the statistical significance. For mono-fractality, the DFA has been used to obtain the scaling Hurst exponent. To characterize the multi-fractality and their possible sources, the MF- DFA is applied to NDVI data sets. Consequently, two are series are generated from the original one: shuffled (random) series and surrogated (phase randomization) [18], [39], [56], [57], [59] The generated series were investigated together with the original and their properties are compared with the original one.

The work is structured as follows: we described the study region, the study domain and data sources. Also, the different measures of correlation (ACF and MF-DFA) which are used in measuring the different measures of correlation (persistence) including their equations are exhaustively discussed in section 2. In section 3, the results and discussions are presented and finally we make our conclusions based on the aim and objectives.

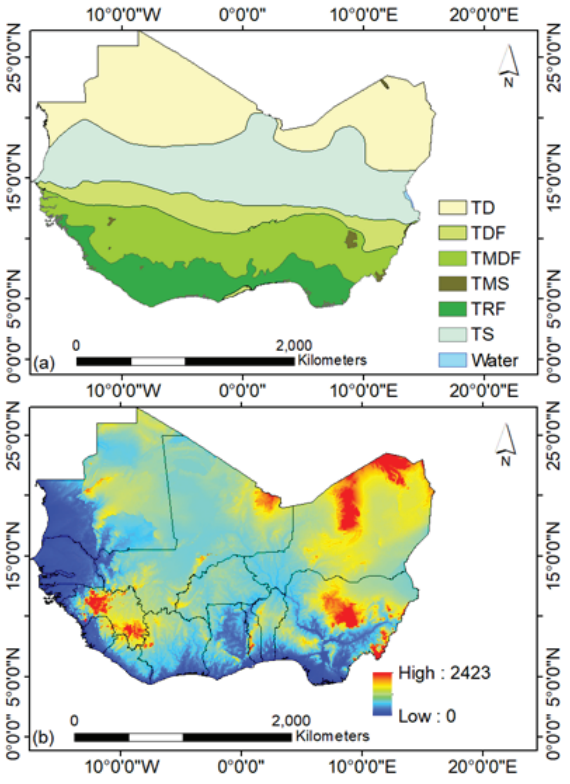

FIGURE 1. Map of West Africa showing (a) ecological regions (FAO, 2000) and (b) Digital Elevation Model (DEM). TD is Tropical Desert, TDF is Tropical Desert Forest, TMDF is Tropical Moist Deciduous Forest, TMS is Tropical Mountain System, TRF is Tropical Rainforest and TS is Tropical Shrubland.

II. MATERIALS AND METHOD

A. STUDY AREA

West Africa comprises of about 16 countries which include; Nigeria, Benin, Togo, Ghana, Ivory Coast, Liberia, Sierra Leone, Guinea, Guinea Bissau, Senegal, Burkina Faso, Cape Verde, Mali, Niger, Mauritania and The Gambia. The region is the most densely populated region in Africa which is located in between the dry Sahel to the north and the Atlantic Ocean to the south and west. The areas close to the ocean are relatively humid [10] and endowed with rich ecosystem while the Sahel is relatively dry and characterized with a rugged terrain (Fig. 1). The plain surface is covered with short, stunted and sparse vegetation. There are a lot of river networks in West Africa and in dry regions of the Sahel,

most settlements are confined to the banks of some rivers or streams. Some natural oases found in the area are often surrounded with vegetation as a result of their higher moisture conditions. West African oases have offered considerable favorable conditions for settlements, trade and transportation routes around the Sahel area. The rainfall in the Guinea (Sahel) region follows a bimodal (unimodal) pattern as a result of the shift in the intertropical convergence zone during the wet season [70]. The West African Monsoon is the main supplier of moisture over the region and the areas close to the Guinea coast are more rain fed compared to the Sahel regions [71], [72]. West Africa has an outlined geography, with subtropical desert ecological regions to the northern border, tropical rain forests in the humid South and Western border and down to the Atlantic Ocean coast. Due to the low elevation around the ocean coast, most rivers over the region shed their waters into the Atlantic Ocean.

B. DATA

This study is based on the Normalized Difference Vegetation index (NDVI) data records obtained from the Global Inventory Modeling and Mapping Studies (GIMMS) third generation third generation (NDVI3g) data records from July 1981 to December 2011 a semi-weekly temporal and 0.083 × 0.083 degrees spatial resolution [73]. The dataset is derived from the NOAA/AVHRR sensors (NOAA 7, 9, 11, 14, 16, 17, 18, and 19), with a spatial resolution of 0.0833 degrees over a 15-day interval. During the extraction of the vegetated areas, pixels with a 30-year averaged NDVI value less than 0.1 were assumed to be non-vegetated and were extracted out [74]. The introduction of satellite remote sensing (RS) in recent decades has proved useful in monitoring vegetation cover changes which using different approaches. Basically, the NDVI is the most frequently used RS vegetation index for vegetation dynamics and degradation observation. NDVI is used to describe the photosynthetic vigor of vegetation [75] and also as an alternative for diverse vegetation properties [76], [77]. Being the only source of long term remote sensing vegetation data, the NDVI retrievals from the NOAA/AVHRRR sensors have contributed a lot in vegetation studies over the Sahel of West Africa and have helped to correct the impression of overstated claims about the desertification extent [78]. The Digital Elevation Model (DEM) was obtained from retrieved from National Aeronautics and Space Administration (NASA) Shuttle Radar Topographic Mission (SRTM) retrieved from http://srtm.csi.cgiar.org/. The data is prepared by Consortium of International Agricultural Research Centers (CGIAR) and has undergone gap filling post-processing of the no data spaces through interpolation techniques. It has a 90 m resolution and the tiles are downloaded as a seamless mosaicked unit at 5 × 5 degrees for easy and convenient usage.

C. METHODS

Fractal methodologies are useful tools for the modelling of complex and stochastic processes. Of important interest is their application in the study of long-range correlation, self-similarity, and the dynamical behavior of non-stationary variables. Persistence in self-affine time series usually is considered when large values are usually followed by large ones and small values are followed by small values. In this work, we considered the Lag-1 Detrendend Autocorrelation Function C (1) and the Multifractal Detrended Fluctuation Analysis (MF-DFA).

1) LAG-1 DETRENDED AUTOCORRELATION (C (1))

The properties of a fractal structure in time series can be measured by the correlation function [41]. Considering equation (1) which is typical of self-similar series, one discovers that it can be either long term correlated, long term anti-correlated or independent [39]. Previous studies [36] have assumed that vegetation time series can be described by Autoregressive processes (AR), and the AR is defined [38], [43] by

$$\vartheta_{i+1} = r_1\vartheta_i + \varepsilon_i, \quad i = 1, 2, \ldots, N-1 \tag{1}$$

where ϑ is the detrended annual mean $(x(t) - \overline{x})$ (usually referred to as random walk) of the NDVI/LAI times series x(t), with local mean $\overline{x}$.r_1 is the AR correlation parameter (−1 to 1) and $\mathcal{E}_i$ the Gaussian white noise. For $r_1 > 0$ and $r_1 < 0$ the series are correlated (persistent) and uncorrelated (anti-persistent) respectively. For $r_1 = 0$, the series shows a Gaussian white noise. The autocorrelation function (ACF) of the linearly detrended record is defined as [21], [38]

$$C(s) = \frac{c(s)'}{\frac{1}{N}\sum_{i=1}^{N}\vartheta(i)^2} \tag{2}$$

$$C(s)' = \frac{1}{N-s}\sum_{i=1}^{N-s}\vartheta(i)\vartheta(i+s) \tag{3}$$

where s is the lag, $C(s)'$ is the auto-covariance. $x(t)$ is uncorrelated, if $c(s) = 0$ (for s > 0) and short term persistent if $C(s)$ deteriorates exponentially according Schumann & Kantelhardt (2011) [43] and Xue *et al.* (2015) [79] as

$$C(s) \propto e^{-s/s_x} \tag{4}$$

where s_x is the decay time [39]. Consequently, for an $AR(1)$ process, $C(1)$ which is the first lag (lag-1) of Eq. (2) is the central quantity [38], so long as N is significantly large enough. A plot of $C(s)$ against S is known as a correlogram and several statistical tests exist that consider N and C (s) for the computed values of S, to evaluate the significance of rejecting the time series as being correlated [43]. For the ACF method, the slope log-log fit of C(s) and s, can also produce the Hurst exponent but due to the fact that the exponential decay of the ACF produces negative values, it is always difficult to evaluate Hurst exponent through log-log fit using the ACF method.

In this work the significance of C (1) was tested using a one-tailed 95% significant test of the Gaussian distribution [80]. It is given by

$$C(1)_t = \frac{-1 \pm \delta_g\sqrt{N-2}}{N-1} \tag{5}$$

where δ_g is the standard deviation in the Gaussian distribution obtained at 95% significance level. Positive and negative values of $c(1)$ represents Markov linear type persistence (correlation) and high frequency respectively [33], [80].

2) MULTIFRACTAL DETRENDED FLUCTUATION ANALYSIS (MF-DFA)

Generally, an MF-DFA algorithm consists of the steps below [37], [39], [42], [44], [56]:

Step 1: We let $x(t)$ be the times series of NDVI for i $= 1, 2, \ldots .N$. Since the integrated series have been obtained using Eq. (10) above, the $x(t)$ is considered to be a random walker (Najafi *et al.*, 2015) that consist of succession of steps around the mean.

Step 2: The integrated series of NDVI is then divided into N_s non-overlapping partitions (bins) given as $N_s = int(N/s)$, where s is the time interval. If N is not a multiple of S, then the technique is repeated out from the opposite end of the series. With this, segments of equal lengths will be $2\,N_s$.

Step 3: then the local trend for each of the $2\,N_s$ segments is estimated by applying a least square fit to the segments. Accordingly, we let y_p to be the best fit to an arbitrary segment p of the series. Thereafter, the variance is determined as [41], [56], [59], [81]:

$$F^2(p, s) = \frac{1}{s}\sum_{i=1}^{s}\left\{Y(i)[(p-1)s+i] - y_p(i)\right\}^2 \quad (6)$$

And, similarly for $p = 1, \ldots .N_s$ and $p = N_s + 1, \ldots 2\,N_s$, the variance is computed as:

$$F^2(p, s) = \frac{1}{s}\sum_{i=1}^{s}\left\{Y(i)\left[(N-(p-N_s)\,s+i\right] - y_p(i)\right\}^2 \quad (7)$$

Step 4: The q^{th} order of the MF-DFA fluctuation is defined by Eqs. (8) and (9)

$$F_q(s) = \left\{\frac{1}{2N_s}\sum_{p=1}^{2N_s}\left[F^2(p, s)\right]^{q/2}\right\}^{1/q}, \quad \text{for } q \neq 0 \quad (8)$$

$$F_q(s) = exp\left\{\frac{1}{4N_s}\sum_{p=1}^{2N_s}\ln\left[F^2(p, s)\right]\right\}, \quad \text{for } q = 0 \quad (9)$$

Step 5: Determine the scaling pattern of the fluctuation function for a range of q moments. When is positive, partitions with large fluctuations will display smaller $h(q)$ while for negative q partitions with small fluctuations will display larger $h(q)$ [56]. And so, if the NDVI and LAI series are long term correlated according to the power law described in Eq. (6), then $F_q(s)$ will increase significantly for large values of S. And then, the generalized Hurst function $h(q)$ will be determined by least square logarithm fit of Eq. (10) [21], [41], [51], [82] below

$$F_q(s) \propto s^{h(q)} \quad (10)$$

Generally, for $h(q) > 0.5$, the series is long range correlated and for $h(q) < 0.5$ the series is long range anti-correlated. If $h(q) = 0.5$, then the series is random (white noise). For $0.5 < h(q) < 1$, the series is considered long term correlated which is a typical behavior of multifractal series and the value of $h(q)$ in the order 2 (i.e., $h(2)$) is similar to the usual Hurst exponent [41], [42]. And $h(2)$ is related to the correlation exponent γ and power spectrum exponent by β [37], [40], [44], [83]:

$$\beta = 1 - \gamma = 2h(2) - 1 \quad (11)$$

Accordingly, for $\beta > 0$ the series are long term correlated while for $\beta < 0$, the series are anti-correlated. If $\beta = 0$, the series are uncorrelated [43].

Specifically, the concept of the classical multifractal scaling exponent $\tau(q)$ can be expressed in terms of the generalized hurst exponent $h(q)$ [39], [56], [59], [81], [84]:

$$\tau(q) = qh(q) - 1 \quad (12)$$

From Eq.(12), the singularity spectrum (spectral function) $f(\alpha)$ can be defined via a Legendre transform $\alpha = (\partial\tau)/(\partial q)$ and $f(\alpha) = q\alpha - \tau(q)$ [39], [42], [50], [83], [84]. Where α is the singularity strength (Holder exponent) [44] and $f(\alpha)$ represents the dimension of the subset series in α. The concept provides clear evidence about the long range correlation in time series. Using Eq. (12) α and $f(\alpha)$ can be expressed in terms of $h(q)$ as [39], [41], [82]:

$$\alpha = h(q) + q\left(h'(q)\right) \quad (13)$$

$$f(\alpha) = q[\alpha - h(q)] + 1 \quad (14)$$

In multifractal analysis, the width (ω) of the singularity spectrum provides a direct measure of the degree of multifractality [56] and it also describes the range of the exponent [37]. ω is given as the difference between the maximum and minimum α, expressed as [35], [37], [51], [56], [81], [83]:

$$\Delta\alpha = \alpha_{max} - \alpha_{min} \quad (15)$$

which satisfies $f(\alpha) \to 0$ for $\alpha \to \alpha_{max}$ and $\alpha \to \alpha_{min}$ [60].

III. RESULTS AND DISCUSSION

A. STATISTICAL CHARACTERISTICS OF NDVI

Figs. 2a, b and c, show the trend, seasonal and irregular (remainder) components of vegetation over West Africa from 1982 to 2011.

The semi-monthly NDVI time series (Y_t) was regarded as an additive series of three components: Trend (T_t), Seasonality (S_t) and Reminder (R_t). The decomposition of the original NDVI series was done according to the equation $Y_t = T_t + S_t + R_t$ [85], and our assumption here is that, NDVI temporal and spatial series are composed of some pattern which is concealed by random noise (or irregularity). The extraction was done in R lab software, according to the STL (weighted regression) method [85] and the extracted trend was used for further analysis. The variation of NDVI over West Africa is highly variable and the fluctuations show a strong trend with slope of 12.4×10^{-4} NDVI/month, with a seasonal range of 0.2 (max amplitude $= -0.1$ and min amplitude $= +0.1$). The standard deviation (SD) of the irregular part is 0.02 while the maximum and the minimum amplitude of the irregular

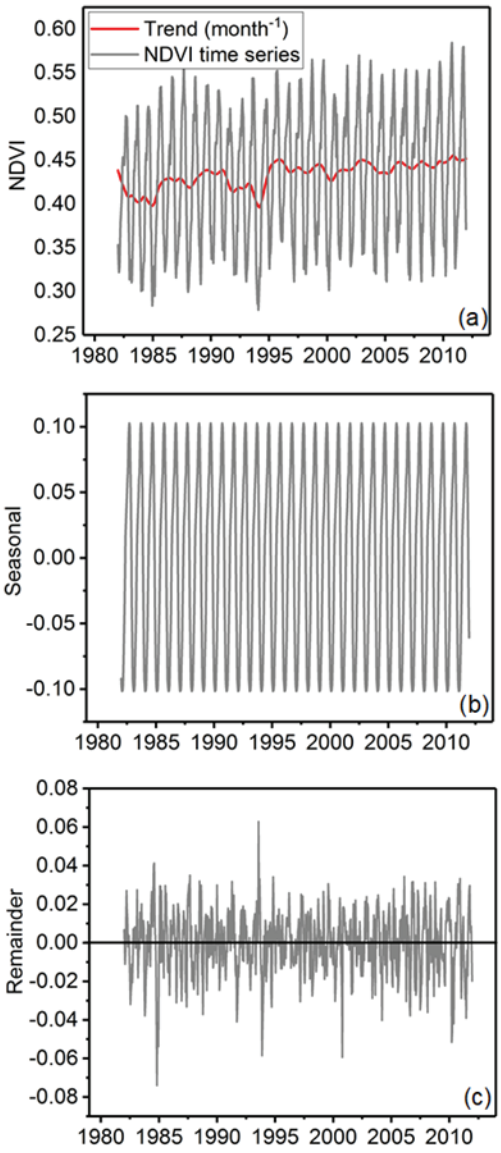

FIGURE 2. NDVI (a) trends, (b) seasonal, and (c) remainder over West Africa from 1982 to 2011.

series are 0.06 and −0.07 respectively. The trend shows a strong non-linear pattern, thus the need to apply non-linear analysis coupled with a power law technique. The Skewness and Kurtosis are −1.22 and −0.08 respectively which means the distribution is not normal. A negative Skewness shows that the series has more response to precipitation during the third quarter of the year (July, August and September summer season) and a negative kurtosis indicates the peak of the series is low. The reason could be that, over West Africa, the vegetation distribution is heterogeneous and the dynamics in vegetation both at temporal and spatial scales are majorly explained by rainfall. The rainfall pattern over Guinea and Sahel regions of West Africa is bi-modal and mono-modal respectively.

Table 1 shows the correlation between NDVI and climate elements over West Africa across the ecological zones. It was

TABLE 1. Correlation between NDVI and climate elements from 1982 to 2011 (Pos. means positive and Neg. means negative).

Eco-Zone	NDV vs Temperature			NDVI vs Precipitation		
	Neg. (%)	Zero (%)	Pos. (%)	Neg. (%)	Zero (%)	Pos. (%)
TD	83	2	15	23	21	57
TDF	96	0	3	0	3	96
TMDF	99	0	1	7	2	90
TMS	10	0	90	0	40	60
TRF	99	0	1	8	4	88
TS	87	2	10	6	1	92

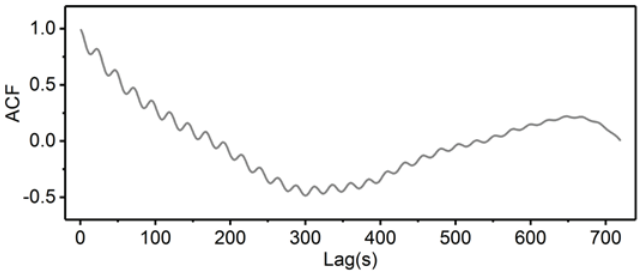

FIGURE 3. Detrended Autocorrelation Function ACF ($C(s)$) of NDVI time series at 15-day time interval (s) over West Africa from 1982 to 2011.

observed that about 57, 96, 90, 60, 88, and 92 % pixels showed positive correlation between NDVI versus precipitation while 21, 3, 2, 40, 4 % pixels showed negative correlation between NDVI and precipitation over TD, TDF, TMDF, TMS, TRF and TS respectively. Also, the correlation between NDVI and temperature showed that about 83, 96, 99, 10 and 99 % pixels were negatively correlated over TD, TDF, TMDF, TMS, TRF and TS ecological zones respectively while about 15, 3, 1, 90, 1 and 10 % pixels were positively correlated across TD, TDF, TMDF, TMS, TRF and TS respectively. This suggests that precipitation is the primary climate element that affects vegetation dynamics over West Africa. For the TMS, the correlation between NDVI and temperature shows that about 90 % pixels correlated positively while 10 % correlated negatively. This is expected because the TMS has different climate modifications from the surrounding environments that tend to affect vegetation since there is variation in temperature with increase in altitude.

B. ANALYSIS OF PERSISTENCE: LAG- 1 DETRENDED AUTOCORRELATION C (1)

From Fig. 3, the semi-monthly (1982 to 2011) NDVI data records shows a serial correlation, with fluctuations from positive to negative values with a delayed version of itself as a function of time lag between them.

Positive lags are from C (1) to $C(174)$ and also from $C(542)$ to $C(719)$, whereas negative lags are from C (175) to C (542). The ACF dampens out at higher lags, suggesting that the relationship at a short time interval is larger than the relation over wider distances. The value of C (1) is 0.989

which is positive and significant at 95% confidence level. This is just a hint that NDVI data records over West Africa are persistent but and this result cannot be completely relied upon due to the exponential decay nature of the ACF. C (1) is used because of the following reasons: (1) various auto-regressive and moving average systems (ARIMA) set out distinctive evidence on the ACF, (2) it is useful in the estimation of statistical significance [38] and (3) it can be used to suggest a suitable model for the time series if they are not random. The statistical significance is essential when one wants to evaluate if the trend changes are perhaps due to anthropogenic origin or not [38] and also to check the nature of short range persistence [80], [86]. Now to suggest a suitable model, we apply the C (1) described in Eq. (4) and for negative C (1) the series can be modelled and considered short range correlated (anti persistent) [33] and for positive C (1), it is long range correlated (persistent) [41], [56], [87]. And if we assume that the vegetation data sets are long-term correlated, C (1) may not be meaningful again and is substituted by a power law exponent called the Hurst. This is because the log-log fit of C (s) against may not be feasible due to the negative values shown by the C (s) (Fig. 3). In this work, the Hurst exponent is applied using power scaling laws and techniques based on the MF-DFA (section C). And if indeed NDVI is persistent, the results will actually be confirmed by the power law method because the method assumes that a relative change in one variable is proportional to the relative change in the other variable, independent of the initial size or length of those variables.

C. ANALYSIS OF PERSISTENCE: DETRENDED FLUCTUATION ANALYSIS (DFA)

The previous subsection points to the fact that C (s), however, is not a viable technique for assessing long-term persistence in NDVI, since the model is strongly affected by finite-size effects, thereby restricting the valid extent of the time span (s) [38], [88]. Thus, we adopt a more dependable model where one estimates the fluctuation function F(s) as previously discussed in Eq. (15). Equations (6-9) from the first four (4) steps under MFDFA procedures give the estimation of Hurst exponent using the DFA method. Fig. 4a shows the spatial distribution of Hurst scaling exponent over West Africa.

The spatial pattern reveals the spatial heterogeneity in the temporal scaling behavior of the NDVI that corresponds to the individual ecological regions. The exponents of the vegetation time series ranged from 0.0 to 1.3 over the period 1982 – 2011 with a standard deviation of 0.18, while those of China vegetation ranged from 0.4843 to 1.2215 with an standard deviation of 0.08 over the period 1982 – 2006 [68]. High values of h are observed over Guinea coast in southern part of Nigeria, Benin, Togo, Ghana, Liberia, Sierra Leone, Senegal and Guinea. Also, high values of h were observe over Sahel in Northeastern Niger, Northern part of Mali, northcentral, northeast and north west of Mauritania. Low to

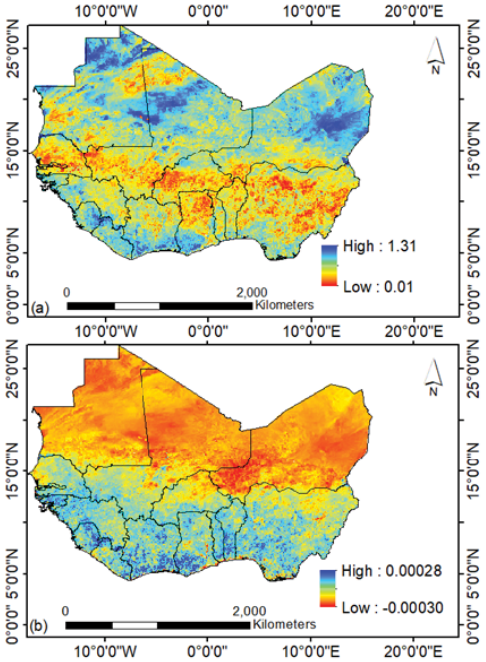

FIGURE 4. Spatial distribution of (a) Hurst exponent using DFA and (b) NDVI trends using OLR from 1982 to 2011.

moderate values of h are observed around the Sudano-Sahel region cutting across Nigeria, Benin, Togo, Ghana, Burkina Faso, Mali, Senegal and parts of Mauritania. This area is basically the grazing corridor characterized by high level of vegetation degradation.

The spatially averaged Hurst exponent over West Africa for 30 years is 0.58 while that of China is 0.78 over a period of 25yrs, which implies China's vegetation is more persistent than West Africa. This is because China has adopted sound ecological development and maintenance programs compared to West Africa. About 37.4, 20.5, 41.7 and 0.5% of the vegetated areas are anti-correlated ($h < 0.5$), un-correlated ($h = 0.5$), correlated ($0.5 < h < 1$) and uncorrelated random walk ($h = 1$) respectively. An insignificant amount of the vegetated are was a non-stationary random walk ($h > 1$). This shows that on average, the overall vegetation of West Africa is weakly-correlated, typical of recovery from random fluctuation due to human and natural factors. These spatial patterns demonstrate the broadness of the temporal scaling behavior of vegetation over West Africa. Areas where high (small) values always follow high (small) ones dominates the forest (desert) vegetation while areas where high (low) values of NDVI do not always follow high (low) ones are clearly visible in between latitude 7 and 15 degrees. Areas with high correlation in the Sahel region are those where vegetation is highly resilient and is adapted to climate and environmental stress.

According to Telesca and Lasaponara (2006) [89], higher persistence changes in vegetation degradation as a result of fire suggests that the ecosystem under research is regulated by

a feedback control which carries out the vegetation recovery. Persistence and long range correlation in vegetation with $h > 0.5$ around the TRF zones of West Africa are as a result of stable forested areas close to the coastal regions while uncorrelated areas of $h < 0.5$ are suggestive of urbanization and forested areas being converted to agricultural lands, $h = 0.5$ are suggestive of thicker forested areas that are converted to fragmented forests. Forest fragmentation reduces habitat, adaptability supply and maintenance through a decline in land area. Over the TD, TDF and TS zones, barren lands conversion to irrigated and croplands have favored vegetation persistence over the area while uncorrelated areas are basically as a result of barren and scattered vegetation. For areas with random (uncorrelated) vegetation scaling properties around TMDF, TRF, TDF and TS zones, it was suggestive that grazing activities and crude agricultural practices were the main causes.

Fig. 4b shows the NDVI trends computed from OLR method and result shows that about 54.3, 0.1 and 45.6% of the vegetated areas are positively, uncorrelated and negatively correlated respectively. Compared with Hurst exponent, the trend method by OLR is effective in describing the fluctuation in vegetation along the slope line and for non-linear systems like vegetation; detailed changes are not completely captured. The OLR shows high trend values in the Southern part of the regional where rainfall is high while low trend values are observed over the Sudano-Sahel region where rainfall is low. The distribution of the pixels follows a latitudinal gradient from North (desert vegetation) to South (forest vegetation).

In Fig. 5a, the correlation C(r) (R^2) between NDVI slope and Hurst exponent is -0.22 (0.05) which shows an insignificant relationship between the two techniques. Figs. 5b & c show the histogram of pixel values from Hurst exponent and NDVI slope. The Hurst exponent pixels are normally distributed and also agree with the central limit theorem compared to the NDVI slope pixels. The limit theorem assumes that the mean approximates a normal Gaussian distribution with a bell curve for any set of variables with large number of independent variables and continuous variable outcomes. Thus, the Hurst exponent distribution represents an unbiased series compared to the NDVI trend distribution.

For a vivid understating of this, we produced scatter plots of Hurst exponents at various elevations and latitudes (Fig. 6) and the result was compared with the NDVI trends.

Fig. 6b shows that in every ecological zone, vegetation is being degraded and expanded and the most anti-persistent location is between latitude 8 to 12 degrees. For the NDVI slope, the pixels are observed to be clustered around the zero slope line with between latitude 13 and 17. From latitude 4 to 12 (16 to 25), the NDVI shows high positive (negative) trends above (below) the zero trend line. Compared with NDVI trends from OLR, the DFA method has better revealed the complexities of West Africa's vegetation dynamics and also present a way of understating their spatial distribution. Based on the trends, vegetation seems to exhibit higher (lower) trend

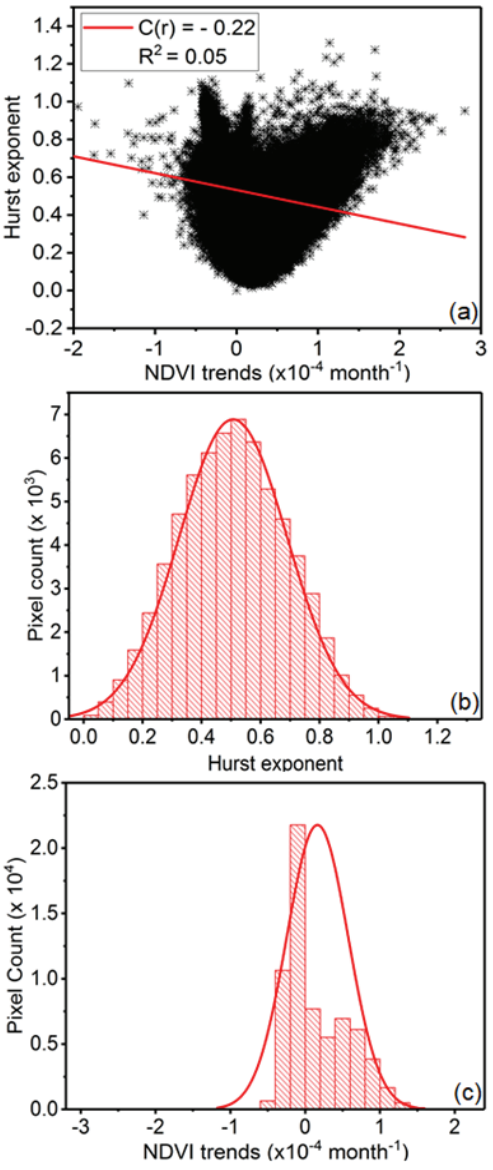

FIGURE 5. (a) Correlation between NDVI slope and DFA Hurst exponent at different grid points; Histogram of pixel values from (b) Hurst exponent and (c) NDVI trends.

changes over the humid forests (arid) regions revealing a zonal symmetry. But, in DFA method, the spatial identification of vegetation changes by Hurst exponent shows variation along the latitudes. This is expected because of the existence of different vegetation cover types in one ecological region, since all the ecological regions are interlaced with each other with no clear sharp boundaries.

In Fig.s 6a & b, the range of Hurst exponent (NDVI trends) in TRF is from 0 to 1.1 (-1.7×10^{-4} to 2.4×10^{-4}) between latitude 4.31 and 11.97 degrees, for TMS the range is from 0.04 to 0.78 (1.35×10^{-5} to 1.38×10^{-4}) located between latitude 6.47 and 11.8 degrees, for TMDF it is from 0 to 1.05 (-1.5×10^{-4} to 2.15×10^{-4}) located between latitude 6.47 and 11.8 degrees, for TDF the range is from 0 to 0.97 (-3×10^{-4} to 2.2×10^{-4}) located between latitude

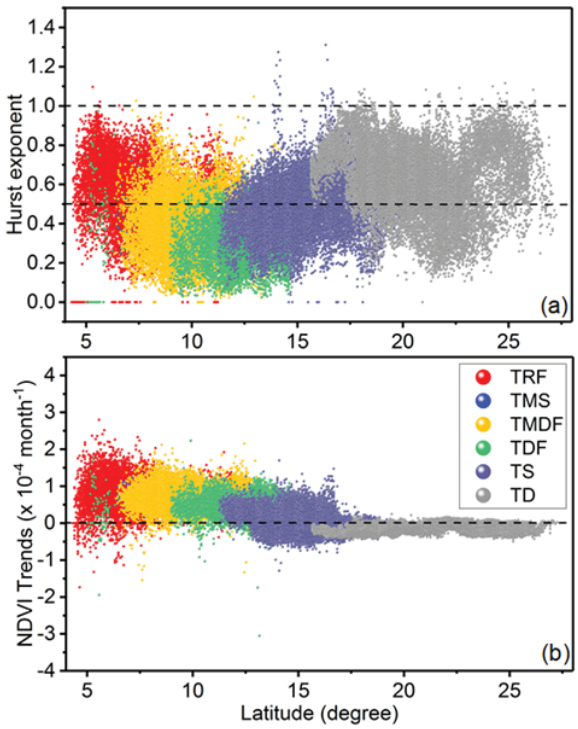

FIGURE 6. Range of (a) DFA Hurst exponents at various latitudes (degrees) and (b) NDVI trends at various latitudes.

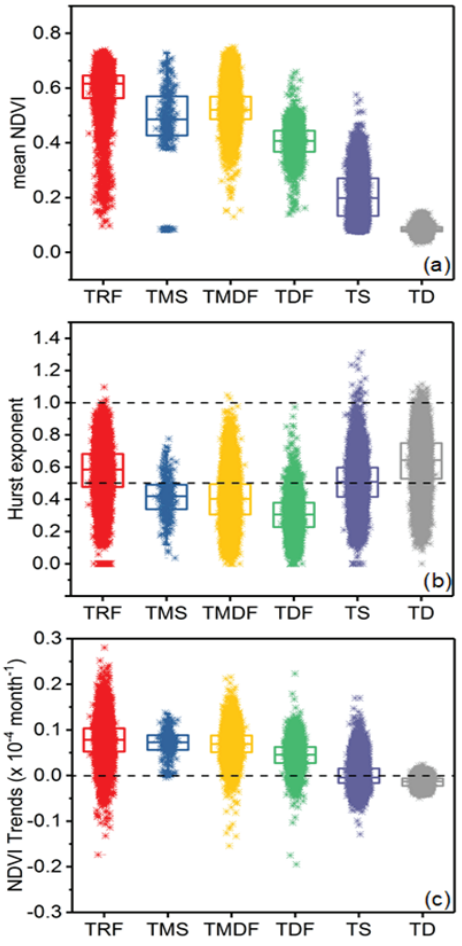

FIGURE 7. Distribution of (a) mean NDVI, (b) DFA Hurst exponent and (c) NDVI slope at various ecological zones.

4.99 and 14.74 degrees, for TS the range is from 0 to 1.31 (-1.3×10^{-4} to 1.7×10^{-4}) located between latitude 11.26 and 20.43 degrees, for TD the range is from 0 to 1.12 (-4.9×10^{-5} to 2.4×10^{-5}) located between latitude 15.67 and 23.33 degrees. The standard deviation (SD) for Hurst exponent (NDVI slope) over TRF, TM, TMDF, TDF, TS and TD is 0.16 (4.11×10^{-4}), 0.12 (2.37×10^{-4}), 0.15 (2.87×10^{-4}), 0.11 (2.77×10^{-4}), 0.14 (2.72×10^{-5}) and 0.17 (1.1×10^{-5}) respectively.

Fig. 7a shows the mean NDVI for various ecological regions and results shows that the TRF (TD) regions exhibit high (low) semi-monthly NDVI values which are above (below) average. There is a decrease in the mean NDVI values from the humid forest to the desert regions. In Fig. 7b, the Hurst exponent display a complex pattern with high clusters located over the TRF, TS and TD ecological zones while moderate and low values are located around the TMDF, TMS, and TDF ecological zones. In the TRF, TMDF, TS and TD zones, high values ($h > 1$) represents regions with non-stationary random walk, which are considered difficult to model and predict as a result of (1) complex changes (2) non availability of data and (3) difficult topography.

Fig. 7c illustrates the NDVI trends in the various ecological zones, and result shows that the mean semi-monthly trends were positive while in TS (TD) the trends were around zero with TS (TD) slightly above (below) zero. Specifically, both the Spatial Hurst exponent and the NDVI slope values have revealed well-defined variability over the study area and revealed high clusters in low elevation areas below 1500 meters (Figs. 1 & 2). But comparison between them shows that the DFA Hurst exponent has been able to capture the little changes and improvements in vegetation over the tropical desert areas compared to the OLR method. Recent studies have shown that the TS and TD which comprises the Sahel have shown remarkable improvement in vegetation in recent decades. Despite strong efforts in research over the Sahel, there is no general agreement about the re-greening of the Sahel and persistent desertification. Thus, this method could be useful in identifying areas with improved and degraded vegetation, which cannot be captured by the OLR method (Figs. 4a & b).

D. MULTIFRACTALITY: MULTIFRACTAL DETRENDED FLUCTUATION ANALYSIS (MF-DFA)

In this section, the multifractal scaling properties of NDVI was investigated using the MF-DFA. DFA was selected because it is minimally affected by record length while the ACF method can be affected by record length variation [33]. The DFA method is a mono-fractal method obtained from the first four steps of the MFDFA, which is insufficient to characterize time series with MF properties. Mono-fractal

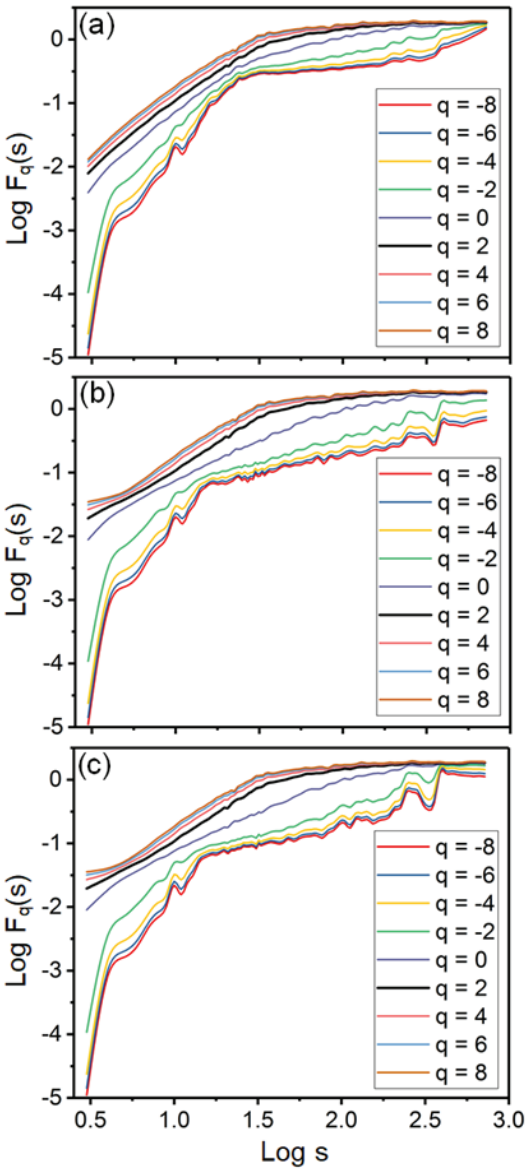

FIGURE 8. MF-DFA results of (a) original (c) Shuffled and (c) Surrogated NDVI from 1982 to 2011.

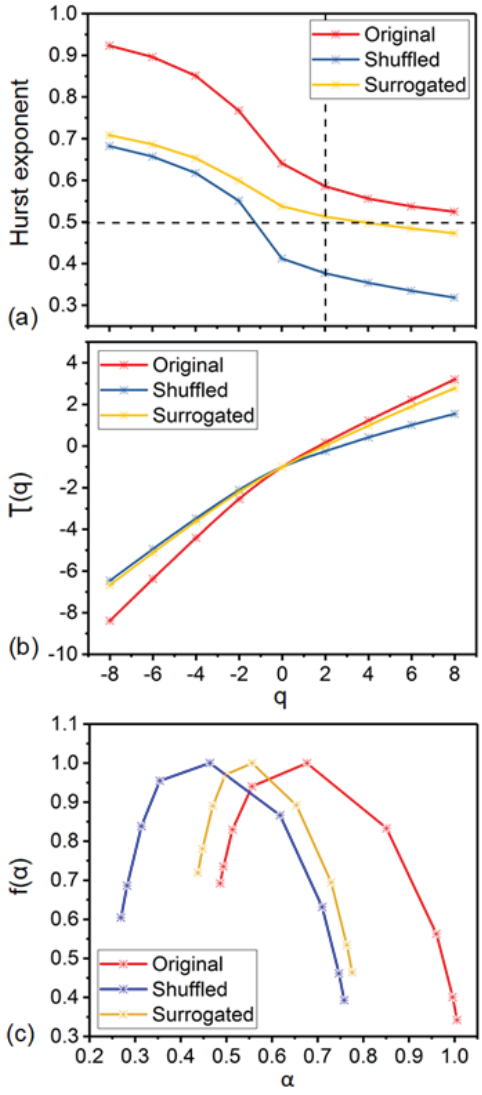

FIGURE 9. The relationship between (a) the generalized Hurst exponent h(q) and q, (b) multi-scaling exponent τ(q) and q, and (c) the multi-fractal spectra exponent f (α) exponent and α NDVI series of West Africa.

methods suppress the multi-fractality of time series and assume that both stationary and nonstationary time series are mono-fractal by indicating a single scaling exponent h [41]. However, NDVI time series are characterized by a lot of irregularities (Fig. 2c) with many complex fractal subsets demonstrating MF scaling property. Equations (6-10) are used in estimating MF in NDVI. Figs. 8a-c show the power-law dependence of log $F_q(s)$ against log s for different orders of q (-8 to 8) with an interval of 2.0. For each time series, $h(q)$ is estimated by the slope of the least square poly fits between the log–log plot of $F_q(s)$ versus log s for each value of q.

Fig. 9a reveals that the generalized Hurst exponent $h(q)$ are decreasing functions that display a strong relationship with each moment q, which suggest that vegetation time series is characterized by MF behavior. The exponent $h(q)$ outlines the scaling behavior of the q^{th} order fluctuation function [59], [87].

According to Tanna and Pathak (2014) [56], the uniqueness of the qth order fluctuation for positive and negative q's from the least segment sizes to the large segment partitions for the both time series indicate the multi-scaling characteristics of considered series. The smaller partitions are able to differentiate between the local time periods with large and small fluctuations (i.e., $-q$ and $+q$'s, respectively) because, smaller segments are enclosed within these time periods. Nevertheless, the large partitions intersect several local time periods with both small and large fluctuations and their fluctuations in magnitude are normalized, the value of h varies on q values and so we deduce that they have a multifractal structure.

Furthermore, the values of the classical multifractal scaling exponent $\tau(q)$ have been calculated using Eq. (12) and multifractal spectrum $f(\alpha)$ have also been calculated through the

Legendre relationship. Generally, the non-linear dependence of the classical scaling exponent $\tau(q)$ on q, is clearly from the relationship between $h(q)$ and q (Figs. 9a & b) [56], which reveals the presence of non-linear interaction between the different scale events and multifractal nature of the vegetation time series.

From Fig. 9c, the resulting multifractal spectra $f(\alpha)$ mimics a characteristic left truncated symmetrical bell with a long right tail, which is an indication that vegetation over West Africa is sensitive to small magnitudes of local fluctuations. Ihlen reported that time series would produce a long left when they are insensitive to local fluctuations of smaller magnitudes, and long right tail when they are insensitive to local fluctuations of larger magnitudes [85]. Eq. (15) was used in computing the absolute width of the multifractal spectrum (ω) for the value of generalized Hurst at $q = 2$ because of the relationship with the well-known Hurst exponent. The width ω and the shape of the multifractal spectrum are related to the changes in $h(q)$ [37], [56], [86]. From Table 2, width ω ($h(q = 2)$) of the NDVI series are obtained as 0.519(0.586). The sporadic fluctuations in vegetation both at small and large scales have been defined by the width of the spectrum.

TABLE 2. Multifractal width ω, Hurst exponent h (2) and multifractal spectrum exponent β.

Type of series	ω	h (2)	β
Original	0.519	0.586	0.172
Shuffled	0.489	0.377	-0.246
Surrogated	0.338	0.513	0.026

Overall, the $MF - DFA$ results show that NDVI is long-range correlated and multi-scaling, the preceding values at any grid point are related to the present values and they also have some effects on both the current and future values. This means that when changes occur in NDVI at the present instance, the changes tend to occur in the next moment. Also, the effect of small and large scale fluctuations is discernible in Fig. 8 for all the records using the value of h (2). By using eye balling method [41], a crossover (about 14 months) point is observed on h (2) in Fig. 9a of the original NDVI series, which is separated by two regimes. The location of the crossover point indicates annual cycle of vegetation, implying strong coupling between climate variables like precipitation and soil moisture.

E. ORIGIN OF MULTIFRACTALITY IN NDVI TIME SERIES OVER WEST AFRICA

To study the complexity of NDVI and LAI due to random correlations in the time series, we performed two analyses on the shuffled and surrogated the original series in comparison with the original series. Specifically, there are two forms of MF, which are due to long range correlations and PDF [39], [56]. The shuffling technique destroys the long range correlation but keeps the original data distribution unchanged, while in the surrogating technique produces phase randomization but preserves the linear properties of the time series like *AFC* [39], [46], [56], [59]. Now we can determine the difference between the Original (h_{org}) and the Shuffle (h_{sh})/Surrogate (h_{sur}) series by considering the differences between these two scaling functions in Eqs. (16) & (17). They can be obtained from the ratio between the fluctuation functions of the original and shuffled/surrogated series which directly shows the presence of long-range correlations or broadness of the PDF in the original series (Tanna & Pathak, 2014). The two ratios are given as [90]

$$\frac{F_q(s)}{F_q sh(s)} \sim s^{h(q)-h_{sh}(q)} = s^{h_{cor}(q)} \tag{16}$$

$$\frac{F_q(s)}{F_q sur(s)} \sim s^{h(q)-h_{sur}(q)} = s^{h_{pdf}(q)} \tag{17}$$

According to Jafari *et al.* (2007) [90], if $h_{sh}(q)$ is random (i.e., 0.5), then the existence of multi-fractality (MF) is due to correlation. And for combined MF due heavy tailed PDF and correlation, $h_{sh}(q)$ and $h_{sur}(q)$ will show dependence on q. But for MF due to heavy tail PDF $h(q) = h_{sh}(q)$ and $h_{cor}(q) = 0$, and for $h_{cor}(q) \neq 0$ MF is suggested to originate from long range correlation [90]. From the Table 1, results show that the values of $h(2)$, ω and β obtained from the original series differed from the shuffled and the surrogated series. It can be noticed that compared with original series, the variation amplitudes of scaling, spectrum and correlation are reduced by means of shuffled and surrogate procedure. We observed that, the spectrum of series of $h(2)$ and ω for NDVI original data series were larger and strongly order dependent than those for shuffled and surrogated series. Also the shuffled and the surrogate series produced β values closer to zero (0) than the original series which depicts that, more noise was introduced during the shuffling and surrogating processes. To check the nature of MF in NDVI series, we considered Eqs. (16) & (17) and results from Table 1 show that the MF properties of NDVI are both from PDF and long range correlation. Arguably, the MF due to long range correlation is dominant. From Fig. 9c, it can be seen that the widest range ($\Delta\alpha$) of the MF spectrum in original, shuffled and surrogated time series is obtained as 0.52, 0.49 and 0.34 respectively, which showed that the strength and complexities of MF in the original series are higher than the shuffled and surrogated series. Also, the values of $\Delta f > 0$, show that longer time scales have more chance of having improved NDVI while the chance of NDVI correlations is higher at a longer time scales compared to lower time scale and vice versa.

IV. CONCLUSION

Many data records in the Earth Sciences indicate long-range correlations and it is very important to determine the strength and source of such correlations. In this work, we analyzed the long range correlations in NDVI data using different methods. The spatial and temporal scaling h values of the well-known Hurst exponent showed that NDVI series are long range correlated. For *ACF*, it was difficult to compute the scaling h values using log-log plots due to the appearance

of negative values in the ACF values, results showed that $C(1)$ value was positive and significant at 95% confidence interval. The spatial pattern of Hurst exponents in NDVI reveals the spatial heterogeneity in the temporal scaling behavior of the NDVI that rhymes with the individual ecological regions. The SD of the exponent is 0.18 and the range is from 0.0 to 1.3 over the period 1982 – 2011, while the range of exponent over China is from 0.4843 to 1.2215 with SD of 0.08 over the period 1982 – 2006 [68]. The spatially averaged exponent over West Africa for 30 years is 0.58 while that of China is 0.78 over a period of 25 years, which implies China's vegetation is more persistent than West Africa. This is because China has adopted sound ecological development and maintenance programs compared to West Africa. About 59.6, 11.3, 29.0 and 0.1% of the vegetated areas over West Africa are anti-correlated, un-correlated (random), correlated and uncorrelated random walk respectively. desert areas reflect the amount of vegetation dynamics which is expressed in terms of the resilience [89].

The exponents display a complex pattern with high clusters located over the TRF and TD ecological zones while moderate and low values are located around the TMDF, TDF, TMS, and TDF ecological zones. A comparison between DFA Hurst exponent and NDVI slope from OLR indicates that the Hurst exponents have been able to capture the little but intermittent changes in vegetation over the TD than the NDVI slope values. The slight improvements (high degradation) in vegetation around the Sahel region have been well noted (see Fig. 4a). Our analyses indicate that not all areas that exhibited negative trends in NDVI slope were long range anti-correlated and vice versa.

The broadness and complexity of the vegetation series was assessed using the $MF-DFA$ method and results showed the existence of prominent MF properties in vegetation records. The q dependence $h(q)$ and $\tau(q)$ in vegetation time series is clearly a fingerprint of MF. Accordingly, by comparing the original series to the shuffled and surrogated one, our analysis indicates that the MF pattern due to long range correlations is dominant in NDVI over West Africa. This shows that MF over the region scale is as a result of self-affine clustering of time patterns of mean vegetation values on different time scales ranging from seasonal to annual. A crossover point at about 14 months can be observed on *h(2)* from the log-log plot in Fig. 9a, which is attributed to a one year (annual) cycle of vegetation, implying strong coupling between climate variables like precipitation and soil moisture.

The presence of long range correlations are therefore helpful in the formulating crop and environmental management policies that may be used to improve ecosystem management using a long term plan (inter-annual) or short term (inter-seasonal) planning. However, the work was restricted by the spatial and temporal resolution of the vegetation (GIMMS AVHRR NDVI 3g) records and it is hoped that in future, longer temporal and finer spatial resolutions may provide a better understanding about the spatial and temporal dynamics of vegetation over the region.

REFERENCES

[1] D. O. Fuller and C. Ottke, "Land cover, rainfall and land-surface albedo in West Africa," *Climatic Change*, vol. 54, nos. 1–2, pp. 181–204, Jul. 2002. doi: 10.1023/A:1015730900622.

[2] Z. Liu, M. C. Wimberly, and F. K. Dwomoh, "Vegetation dynamics in the upper guinean forest region of West Africa from 2001 to 2015," *Remote Sens.*, vol. 9, no. 1, p. 5, 2017. doi: 10.3390/rs9010005.

[3] C. Spinage, *African Ecology Benchmarks and Historical Perspectives*. London, U.K.: Springer, 2012. doi: 10.1007/978-3-642-22872-8.

[4] S. E. Nicholson, C. J. Tucker, and M. B. Ba, "Desertification, drought, and surface vegetation: An example from the West African Sahel," *Bull. Amer. Meteorolog. Soc.*, vol. 79, no. 5, pp. 815–830, May 1998. doi: 10.1175/1520-0477(1998)079<0815:DDASVA>2.0.CO;2.

[5] M. Mortimore and B. Turner, "Does the Sahelian smallholder's management of woodland, farm trees, rangeland support the hypothesis of human-induced desertification?" *J. Arid Environ.*, vol. 63, no. 3, pp. 567–595, Nov. 2005. doi: 10.1016./j.jaridenv.2005.03.005.

[6] L. Olsson, L. Eklundh, and J. Ardö, "A recent greening of the Sahel–Trends, patterns and potential causes," *J. Arid Environ.*, vol. 63, no. 3, pp. 556–566, Nov. 2005. doi: 10.1016/j.jaridenv.2005.03.008.

[7] R. Wittig, K. König, M. Schmidt, and J. Szarzynski, "A study of climate change and anthropogenic impacts in West Africa," *Environ. Sci. Pollut. Res.-Int.*, vol. 14, no. 3, pp. 182–189, May 2007. doi: 10.1065/espr2007.02.388.

[8] O. A. Abdi, E. K. Glover, and O. Luukkanen, "Causes and impacts of land degradation and desertification: Case study of the Sudan," *Int. J. Agricult. Forestry*, vol. 3, no. 2, pp. 40–51, 2013. doi: 10.5923/j.ijaf.20130302.03.

[9] A. Bamba, B. Dieppois, A. Konaré, T. Pellarin, A. Balogun, N. Dessay, B. Kamagate, I. Savané, A. Diedhiou, "Changes in vegetation and rainfall over west africa during the last three decades (1981-2010)," *Atmos. Climate Sci.*, vol. 5, no. 5, pp. 367–379, Jun. 2015. doi: 10.4236/acs.2015.54028.

[10] C. Cabot. (2016). *Climate Change, Security Risks and Conflict Reduction in Africa: A Case Study of Farmer-Herder Conflicts Over Natural Resources in Côte d'Ivoire, Ghana and Burkina Faso 1960-2000*. [Online]. Available: https://www.google.com.ng/webhp?sourceid=chrome-instant&ion=1&espv=2&ie=UTF-8&client=ubuntu#q=Part+A:+Global+and+Sectoral+Aspects.+Contribution+of+Working+Group+II+to+the+Fifth+Assessment+Report+of+the+Intergovernmental+Panel+on+in+Climate+Change&

[11] S. Scheiter and P. Savadogo, "Ecosystem management can mitigate vegetation shifts induced by climate change in West Africa," *Ecolog. Model.*, vol. 332, pp. 19–27, Jul. 2016. doi: 10.1016/j.ecolmodel.2016.03.022.

[12] S. M. Herrmann and C. F. Hutchinson, "The changing contexts of the desertification debate," *J. Arid Environ.*, vol. 63, no. 3, pp. 538–555, Nov. 2005. doi: 10.1016/j.jaridenv.2005.03.003.

[13] T. Igbawua, J. Zhang, Q. Chang, and F. Yao, "Vegetation dynamics in relation with climate over Nigeria from 1982 to 2011," *Environ. Earth Sci.*, vol. 75, p. 518, Mar. 2016. doi: 10.1007/s12665-015-5106-z.

[14] C. A. Alo and G. Wang, "Role of dynamic vegetation in regional climate predictions over Western Africa," *Climate Dyn.*, vol. 35, no. 5, pp. 907–922, Oct. 2010. doi: 10.1007/s00382-010-0744-z.

[15] A. Dai, "Drought under global warming: A review," *Wiley Interdiscipl. Rev., Climate Change*, vol. 2, no. 1, pp. 45–65, Jan./Feb. 2011. doi: 10.1002/wcc.81.

[16] R. J. Hobbs and H. A. Mooney, *Remote Sensing of Biosphere Functioning, Ecology Studies*, vol. 79. New York, NY, USA: Springer-Verlag, 1990. doi: 10.1002/joc.3370110411.

[17] L. A. Martín-Montoya, N. M. Aranda-Camacho, and C. J. Quimbay, "Long-range correlations and trends in Colombian seismic time series," *Phys. A, Stat. Mech. Appl.*, vol. 421, pp. 124–133, Mar. 2015. doi: 10.1016/j.physa.2014.10.073.

[18] W. Chen, T. Sakai, K. Moriya, L. Koyama, and C. Cao, "Estimation of vegetation coverage in semi-arid sandy land based on multivariate statistical modeling using remote sensing data," *Environ. Model. Assessment*, vol. 18, no. 5, pp. 547–558, Oct. 2013. doi: 10.1007/s10666-013-9359-1.

[19] X. Cui, C. Gibbes, J. Southworth, and P. Waylen, "Using remote sensing to quantify vegetation change and ecological resilience in a semi-arid system," *Land*, vol. 2, no. 2, pp. 108–130, Mar. 2013. doi: 10.3390/land2020108.

[20] A. A. Gitelson, Y. J. Kaufman, R. Stark, and D. Rundquist, "Novel algorithms for remote estimation of vegetation fraction," *Remote Sens. Environ.*, vol. 80, no. 1, pp. 76–87, Jun. 2001. doi: 10.1016/S0034-4257(01)00289-9.

[21] F. Wang, G.-P. Liao, X.-Y. Zhou, and W. Shi, "Multifractal detrended cross-correlation analysis for power markets," *Nonlinear Dyn.*, vol. 72, nos. 1–2, pp. 353–363, Apr. 2013. doi: 10.1007/s11071-012-0718-2.

[22] M. Robin, J.-L. Chapuis, and M. Lebouvier, "Remote sensing of vegetation cover change in islands of the Kerguelen archipelago," *Polar Biol.*, vol. 34, no. 11, pp. 1689–1700, Nov. 2011. doi: 10.1007/s00300-011-1069-z.

[23] L. Telesca, R. Lasaponara, and A. Lanorte, "Intra-annual dynamical persistent mechanisms in Mediterranean ecosystems revealed SPOT-VEGETATION time series," *Ecolog. Complex.*, vol. 5, no. 2, pp. 151–156, Jun. 2008. doi: 10.1016/j.ecocom.2007.10.001.

[24] G. Jiapaer, S. Liang, Q. Yi, and J. Liu, "Vegetation dynamics and responses to recent climate change in Xinjiang using leaf area index as an indicator," *Ecolog. Indicators*, vol. 58, pp. 64–76, Nov. 2015. doi: 10.1016/j.ecolind.2015.05.036.

[25] D. Xu and X. Guo, "Some insights on grassland health assessment based on remote sensing," *Sensors*, vol. 15, no. 2, pp. 3070–3089, Jan. 2015. doi: 10.3390/s150203070.

[26] P. Villa, M. Boschetti, J. L. Morse, and N. Politte, "A multitemporal analysis of tsunami impact on coastal vegetation using remote sensing: A case study on Koh Phra Thong Island, Thailand," *Natural Hazards*, vol. 64, no. 1, pp. 667–689, Oct. 2012. doi: 10.1007/s11069-012-0261-y.

[27] A. Lausch, M. Pause, I. Z. S. Merbach, D. Doktor, M. Volk, and R. Seppelt, "A new multiscale approach for monitoring vegetation using remote sensing-based indicators in laboratory, field, and landscape," *Environ. Monit. Assessment*, vol. 185, no. 2, pp. 1215–1235, Feb. 2013. doi: 10.1007/s10661-012-2627-8.

[28] L. Liu, X. Jing, J. Wang, and C. Zhao, "Analysis of the changes of vegetation coverage of western Beijing mountainous areas using remote sensing and GIS," *Environ. Monit. Assessment*, vol. 153, nos. 1–4, pp. 339–349, Jun. 2009. doi: 10.1007/s10661-008-0360-0.

[29] J. Rogan, J. Franklin, and D. A. Roberts, "A comparison of methods for monitoring multitemporal vegetation change using Thematic Mapper imagery," *Remote Sens. Environ.*, vol. 80, no. 1, pp. 143–156, Apr. 2002. doi: 10.1016/S0034-4257(01)00296-6.

[30] B. Martínez and M. A. Gilabert, "Vegetation dynamics from NDVI time series analysis using the wavelet transform," *Remote Sens. Environ.*, vol. 113, no. 9, pp. 1823–1842, Sep. 2009. doi: 10.1016/j.rse.2009.04.016.

[31] Z. Cai and X. Wang, "Research on vegetation dynamic change simulation based on spatial data mining of ANN-CA model using time series of remote sensing images," in *Computer and Computing Technologies in Agriculture III*, vol. 317, D. Li and C. Zhao, Eds. Berlin, Germany: Springer, 2010.

[32] F. Geerts and C. Blondia, *Superposition of Markov sources and long range dependence*, U. Kuhn, Ed. London, U.K.: Chapman & Hall, 1998.

[33] A. V. Coronado and P. Carpena, "Size effects on correlation measures," *J. Biol. Phys.*, vol. 31, no. 1, pp. 121–133, Jan. 2005. doi: 10.1007/s10867-005-3126-8.

[34] D. Li, Y. Nishimura, and M. Men, "Why the long-term auto-correlation has not been eliminated by arbitragers: Evidences from NYMEX," *Energy Econ.*, vol. 59, pp. 167–178, Sep. 2016. doi: 10.1016/j.eneco.2016.08.006.

[35] S. Shadkhoo and G. R. Jafari, "Multifractal detrended cross-correlation analysis of temporal and spatial seismic data," *Eur. Phys. J. B.*, vol. 72, no. 4, pp. 679–683, Dec. 2009. doi: 10.1140/epjb/e2009-00402-2.

[36] A. Fernández-Manso, C. Quintano, and O. Fernández-Manso, "Forecast of NDVI in coniferous areas using temporal ARIMA analysis and climatic data at a regional scale," *Int. J. Remote Sens.*, vol. 32, no. 6, pp. 1595–1617, Nov. 2011. doi: 10.1080/01431160903586765.

[37] E. Koscielny-Bunde, J. W. Kantelhardt, P. Braun, A. Bunde, and S. Havlin, "Long-term persistence and multifractality of river runoff records: Detrended fluctuation studies," *J. Hydrol.*, vol. 322, nos. 1–4, pp. 120–137, May 2006. doi: 10.1016/j.jhydrol.2005.03.004.

[38] Y. Wang, D. Zhou, A. Bunde, and S. Havlin, "Testing reanalysis data sets in Antarctica: Trends, persistence properties, and trend significance," *J. Geophys. Res., Atmos.*, vol. 121, no. 21, pp. 12839–12855, Nov. 2016. doi: 10.1002/2016JD024864.

[39] Kantelhardt, J. W, "Fractal & multifractal time series," in *Encyclopedia of Complexity and Systems Science*, vol. 59. 2008. doi: 10.1007/SpringerReference_60393.

[40] P. Varotsos, N. V. Sarlis, and E. S. Skordas, *Natural Time Analysis: The New View of Time*, P. Blondel and C. Geol, Eds. London, U.K.: Springer, 2011. doi: 10.1007/978-3-642-16449-1.

[41] E. Ge and Y. Leung, "Detection of crossover time scales in multifractal detrended fluctuation analysis," *J. Geograph. Syst.*, vol. 15, no. 2, pp. 115–147, Apr. 2013. doi: 10.1007/s10109-012-0169-9.

[42] J. W. Kantelhardt, S. A. Zschiegner, E. Koscielny-Bunde, S. Havlin, A. Bunde, and H. E. Stanley, "Multifractal detrended fluctuation analysis of nonstationary time series," *Phys. A, Stat. Mech. Appl.*, vol. 316, nos. 1–4, pp. 87–114, Dec. 2002. doi: 10.1016/S0378-4371(02)01383-3.

[43] A. Witt and B. D. Malamud, "Quantification of long-range persistence in geophysical time series: Conventional and benchmark-based improvement techniques," *Surv. Geophys.*, vol. 34, no. 5, pp. 541–651, Sep. 2013. doi: 10.1007/s10712-012-9217-8.

[44] A. Y. Schumann and J. W. Kantelhardt, "Multifractal moving average analysis and test of multifractal model with tuned correlations," *Phys. A, Stat. Mech. Appl.*, vol. 390, no. 14, pp. 2637–2654, Jul. 2011. doi: 10.1016/j.physa.2011.03.002.

[45] R. Bartsch, M. Plotnik, J. W. Kantelhardt, S. Havlin, N. Giladi, and J. M. Hausdorff, "Fluctuation and synchronization of gait intervals and gait force profiles distinguish stages of Parkinson's disease," *Phys. A, Stat. Mech. Appl.*, vol. 383, no. 2, pp. 455–465, Sep. 2007. doi: 10.1016/j.physa.2007.04.120.

[46] M. Onderka, L. Mrafková, A. Krein, and L. Hoffmann, "Long-term persistence of stream nitrate concentrations (memory effect) inferred from spectral analysis and detrended fluctuation analysis," *Water, Air, Soil Pollut.* , vol. 223, no. 1, pp. 241–252, Jan. 2012. doi: 10.1007/s11270-011-0854-1.

[47] E. Najafi and A. H. Darooneh, "Long range dependence in texts: A method for quantifying coherence of text," *Knowl.-Based Syst.*, vol. 133, pp. 33–42, Oct. 2015. doi: 10.1016/j.knosys.2017.06.032.

[48] J. Alvarez-Ramirez, E. Rodríguez, and J. C. Echeverría, "Fractal scaling behavior of heart rate variability in response to meditation techniques," *Chaos, Solitons Fractals*, vol. 99, pp. 57–62, Jun. 2017. doi: 10.1016/j.chaos.2017.03.026.

[49] L. Kristoufek, "Fractal approach towards power-law coherency to measure cross-correlations between time series," *Commun. Nonlinear Sci. Numer. Simul.*, vol. 50, pp. 193–200, Sep. 2017. doi: 10.1016/j.cnsns.2017.02.018.

[50] M. Tarafder, P. Sinha, A. Kundu, M. Strangwood, and C. Davis, "Fractal based correlations for Nb microalloyed steel undergoing static recrystallization," *Mater. Characterization*, vol. 85, pp. 92–99, Nov. 2013. doi: 10.1016/j.matchar.2013.08.013.

[51] H.-D. He, J.-L. Wang, H.-R. Wei, C. Ye, and Y. Ding, "Fractal behavior of traffic volume on urban expressway through adaptive fractal analysis," *Phys. A, Stat. Mech. Appl.*, vol. 443, pp. 518–525, Feb. 2016. doi: 10.1016/j.physa.2015.10.004.

[52] D. Mondal, P. N. S. Roy, and P. K. Behera, "Use of correlation fractal dimension signatures for understanding the overlying strata dynamics in Longwall coal mines," *Int. J. Rock Mech. Mining Sci.*, vol. 91, pp. 210–221, Jan. 2017. doi: 10.1016/j.ijrmms.2016.11.019.

[53] A. A. Chernyshov, B. V. Kozelov, and M. M. Mogilevsky, "Study of auroral ionosphere using percolation theory and fractal geometry," *J. Atmos. Sol.-Terr. Phys.*, vol. 161, pp. 127–133, Aug. 2017. doi: 10.1016/j.jastp.2017.06.013.

[54] B. Qian and K. Rasheed, "Hurst exponent and financial market predictability," in *Proc. 2nd IASTED Int. Conf. Financial Eng. Appl.*, 2004, pp. 203–209. [Online]. Available: http://citeseerx.ist.psu.edu/viewdoc/download?doi=10.1.1.137.207&rep=rep1&type=pdf

[55] R. Liu, L. Yu, Y. Jiang, Y. Wang, and B. Li, "Recent developments on relationships between the equivalent permeability and fractal dimension of two-dimensional rock fracture networks," *J. Natural Gas Sci. Eng.*, vol. 45, pp. 771–785, Sep. 2017. doi: 10.1016/j.jngse.2017.06.013

[56] H. J. Tanna and K. N. Pathak, "Multifractality due to long-range correlation in the L-band ionospheric scintillation S_4 index time series," *Astrophys. Space Sci.*, vol. 350, no. 1, pp. 47–56, Mar. 2014. doi: 10.1007/s10509-013-1742-5.

[57] H. Cheng, J.-B. Huang, Y.-Q. Guo, and X.-H. Zhu, "Long memory of price–volume correlation in metal futures market based on fractal features," *Trans. Nonferrous Met. Soc. China*, vol. 23, no. 10, pp. 3145–3152, Oct. 2013. doi: 10.1016/S1003-6326(13)62845-9.

[58] B. Kim, H. Kim, and S.-H. Min, "Hurst's memory for chaotic, tree ring, and SOI series," *Appl. Math.*, vol. 5, no. 1, pp. 175–195, Jan. 2014.

[59] P. Mali, "Multifractal characterization of global temperature anomalies," *Theor. Appl. Climatol.*, vol. 121, nos. 3–4, pp. 641–648, Aug. 2015. doi: 10.1007/s00704-014-1268-y.

[60] M. Dai, J. Hou, and D. Ye, "Multifractal detrended fluctuation analysis based on fractal fitting: The long-range correlation detection method for highway volume data," *Phys. A, Stat. Mech. Appl.*, vol. 444, pp. 722–731, Feb. 2016. doi: 10.1016/j.physa.2015.10.073.

[61] Y. Yuan, X.-T. Zhuang, X. Jin, and W.-Q. Huang, "Stable distribution and long-range correlation of brent crude oil market," *Phys. A, Stat. Mech. Appl.*, vol. 413, pp. 173–179, Nov. 2014. doi: 10.1016/j.physa.2014.06.064.

[62] M. Li and J.-Y. Li, "Generalized cauchy model of sea level fluctuations with long-range dependence," *Phys. A, Stat. Mech. Appl.*, vol. 484, pp. 309–335, Oct. 2017. doi: 10.1016/j.physa.2017.04.130.

[63] L. D. Saein and P. Afzal, "Correlation between Mo mineralization and faults using geostatistical and fractal modeling in porphyry deposits of Kerman magmatic belt, SE Iran," *J. Geochem. Explor.*, vol. 181, pp. 333–343, Oct. 2017. doi: 10.1016/j.gexplo.2017.06.014.

[64] Z. Song, D. Huang, S. Masae, Y. Wang, T. Shigeo, Y. Hori, Y. Yasuo, and J. Chen, "Fractals in spatial patterns of vegetation formations," *Tsinghua Sci. Technol.*, vol. 11, no. 4, pp. 462–469, Aug. 2006. doi: 10.1016/S1007-0214(06)70218-8.

[65] Y. Fu, F. H. Yu, and M. Dong, "Scale-dependent spatial heterogeneity of vegetation in Mu Us sandy land, a semi-arid area of China," *Plant Ecol.*, vol. 162, no. 1, pp. 135–142, Sep. 2013.

[66] S.-W. Zhao, S. Jing, Y.-H. Yang, L. Na-Na, J.-S. Wu, and Z.-P. Shangguan, "A fractal method of estimating soil structure changes under different vegetations on Ziwuling mountains of the loess plateau, China," *Agricult. Sci. China*, vol. 5, no. 7, pp. 530–538, Jul. 2006. [Online]. Available: http://ac.els-cdn.com/S1671292706600886/1-s2.0-S1671292706600886-main.pdf?_tid=04a8b41e-7f4a-11e7-9a51-00000aab0f26&acdnat=1502534334_9837558196cb7d229f1bbf5ad9aa2e9e

[67] X. Guo, D. Liu, and H. Zhang, "Detection of long-range correlation in NDVI over greater Khingan mountains," *J. Geo-Inf. Sci.*, vol. 15, no. 1, pp. 152–158, 2013. doi: 10.3724/SP.J.1047.2013.00152.

[68] X. Guo, H. Zhang, T. Yuan, J. Zhao, and Z. Xue, "Detecting the temporal scaling behavior of the normalized difference vegetation index time series in China using a detrended fluctuation analysis," *Remote Sens.*, vol. 7, no. 10, pp. 12942–12960, Sep. 2015. doi: 10.3390/rs71012942.

[69] X. Zheng and E. A. B. Eltahir, "The role of vegetation in the dynamics of west African monsoons," *J. Climate*, vol. 11, pp. 2078–2096, Aug. 1998. [Online]. Available: http://www.mit.edu/ eltahir/a_jcli98_files/1998 Zheng Eltahir role vegetation JClimate.pdf

[70] M. I. Lélé and P. J. Lamb, "Variability of the intertropical front (ITF) and rainfall over the West African Sudan–Sahel zone," *J. Climate*, vol. 23, no. 14, pp. 3984–4004, Jul. 2010. doi: 10.1175/2010JCLI3277.1.

[71] R. J. Cornforth, "West African monsoon 2012," *Weather*, vol. 68, no. 10, pp. 256–263, Oct. 2013. doi: 10.1002/wea.2161.

[72] R. G. J. Fitzpatrick, C. L. Bain, P. Knippertz, J. H. Marsham, and D. J. Parker, "The West African monsoon onset: A concise comparison of definitions," *J. Climate*, vol. 28, no. 22, pp. 8673–8694, Nov. 2015. doi: 10.1175/JCLI-D-15-0265.1.

[73] M. Forkel, N. Carvalhais, J. Verbesselt, M. D. Mahecha, C. S. R. Neigh, and M. Reichstein, "Trend Change detection in NDVI time series: Effects of inter-annual variability and methodology," *Remote Sens.*, vol. 5, no. 5, pp. 2113–2144, Apr. 2013. doi: 10.3390/rs5052113.

[74] G. Xu, H. Zhang, B. Chen, H. Zhang, J. L. Innes, G. Wang, J. Yan, Y. Zheng, Z. Zhu, and R. B. Myneni, "Changes in vegetation growth dynamics and relations with climate over China's landmass from 1982 to 2011," *Remote Sens.*, vol. 6, no. 4, pp. 3263–3283, Mar. 2014. doi: 10.3390/rs6043263.

[75] R. B. Myneni, F. G. Hall, P. J. Sellers, and A. L. Marshak, "The interpretation of spectral vegetation indexes," *IEEE Trans. Geosci. Remote Sens.*, vol. 33, no. 2, pp. 481–486, Mar. 1995.

[76] A. Anyamba and C. J. Tucker, "Analysis of Sahelian vegetation dynamics using NOAA-AVHRR NDVI data from 19810–2003," *J. Arid Environ.*, vol. 63, no. 3, pp. 596–614, Nov. 2005. doi: 10.1016/j.jaridenv.2005.03.007.

[77] Y. Bai, J. Zhang, S. Zhang, U. A. Koju, F. Yao, and T. Igbawua, "Using precipitation, vertical root distribution, and satellite-retrieved vegetation information to parameterize water stress in a Penman-Monteith approach to evapotranspiration modeling under mediterranean climate," *J. Adv. Model. Earth Syst.*, vol. 9, no. 1, pp. 168–192, Mar. 2017. doi: 10.1002/2016MS000702.

[78] S. M. Herrmann and T. K. Sop, *The Map Is Not the Territory: How Satellite Remote Sensing and Ground Evidence Have Re-shaped the Image of Sahelian Desertification*. Berlin, Germany: Springer, 2016, pp. 117–145. doi: 10.1007/978-3-642-16014-1_5.

[79] Y. Xue, L.-S. Jia, W.-Z. Teng, and W.-Z. Lu, "Long-range correlations in vehicular traffic flow studied in the framework of Kerner's three-phase theory based on rescaled range analysis," *Commun. Nonlinear Sci. Numer. Simul.*, vol. 22, nos. 1–3, pp. 285–296, May 2015. doi: 10.1016/j.cnsns.2014.09.017.

[80] P. Jagannathan and B. Parthasarathy, "Trends and periodicities of rainfall over India," *Monthly Weather Rev.*, vol. 101, no. 4, pp. 371–375, 1973. doi: 10.1175/1520-0493(1973)101<0371:TAPORO>2.3.CO;2.

[81] S. K. Seo, K. Kim, K.-H. Chang, Y.-J. Choi, K. Song, and J.-K. Park, "Determination of the dynamical behavior of rainfalls by using a multifractal detrended fluctuation analysis," *J. Korean Phys. Soc.*, vol. 61, no. 4, pp. 658–661, Aug. 2012. doi: 10.3938/jkps.61.658.

[82] M. Chatzigeorgiou, V. Constantoudis, F. Diakonos, K. Karamanos, C. Papadimitriou, M. Kalimeri, and H. Papageorgiou, "Multifractal correlations in natural language written texts: Effects of language family and long word statistics," *Phys. A, Stat. Mech. Appl.*, vol. 469, pp. 173–182, Mar. 2017. doi: 10.1016/j.physa.2016.11.028.

[83] S. Drozdz, P. Oświęcimka, A. Kulig, J. Kwapień, K. Bazarnik, I. Grabska-Gradzińska, J. Rybicki, and M. Stanuszek, "Quantifying origin and character of long-range correlations in narrative texts," *Inf. Sci.*, vol. 331, pp. 32–44, Feb. 2016. doi: 10.1016/j.ins.2015.10.023.

[84] C. Xue, P. Shang, and W. Jing, "Multifractal Detrended cross-correlation analysis of BVP model time series," *Nonlinear Dyn.*, vol. 69, nos. 1–2, pp. 263–273, Jul. 2012. doi: 10.1007/s11071-011-0262-5.

[85] E. Li, X. Mu, G. Zhao, and G. Peng, "Multifractal detrended fluctuation analysis of streamflow in the yellow river basin, China," *Water*, vol. 7, no. 4, pp. 1670–1686, Apr. 2015. doi: 10.3390/w7041670.

[86] M. Q. Mirza, R. A. Warrick, N. J. Ericksen, and G. J. Kenny, "Trends and persistence in precipitation in the Ganges, Brahmaputra and Meghna river basins," *Hydrolog. Sci. J.*, vol. 43, no. 6, pp. 845–858, Feb. 1998. doi: 10.1080/02626669809492182.

[87] A. Bashan, R. Bartsch, J. W. Kantelhardt, and S. Havlin, "Comparison of detrending methods for fluctuation analysis," *Phys. A, Stat. Mech. Appl.*, vol. 387, no. 21, pp. 5080–5090, Sep. 2008. doi: 10.1016/j.physa.2008.04.023.

[88] D. Chakraborty and J. K. Bhattacharjee, "Finite-size effect in persistence in random walks," *Phys. Rev. E, Stat. Phys. Plasmas Fluids Relat. Interdiscip. Top.*, vol. 75, no. 1, Jan. 2007, Art. no. 011111. doi: 10.1103/PhysRevE.75.011111.

[89] L. Telesca and R. Lasaponara, "Pre- and post-fire behavioral trends revealed in satellite NDVI time series," *Geophys. Res. Lett.*, vol. 33, no. 14, Jul. 2006, Art. no. L14401.

[90] G. R. Jafari, P. Pedram, and L. Hedayatifar, "Long-range correlation and multifractality in Bach's Inventions pitches," *J. Stat. Mech., Theory Exp.*, vol. 2007, no. 4, 2007, Art. no. P04012. doi: 10.1088/1742-5468/2007/04/P04012.

TERTSEA IGBAWUA was born in Gboko, Nigeria, in 1981. He received the B.S. and M.Sc. degrees in physics from Benue State University, Makurdi, Nigeria, in 2006 and 2008, respectively, and the Ph.D. degree from the Institute of Remote Sensing and Digital Earth (RADI), Chinese Academy of Sciences (CAS), China.

Since 2018, he has been a Postdoctoral Researcher with the Remote Sensing Information and Digital Earth Center, College of Computer Science and Technology, Qingdao University, Qingdao, China. Since 2012, he has been a Lecturer with the University of Agriculture, Nigeria. He has authored more than ten articles. His research interests include remote sensing, GIS, vegetation and climate change, environmental and radiation physics, and cartography.

JIAHUA ZHANG received the Ph.D. degree from the Institute of Remote Sensing Applications, Chinese Academy of Sciences (CAS) in Cartography and Remote Sensing, Beijing, China, in 1998.

From 1999 to 2001, he held a postdoctoral position at the National Institute for Environmental Studies, Japan. Since January 2002, he has been a Professor with the Chinese Academy of Meteorological Sciences. Since 2012, he has been a Full Professor with the Institute of Remote Sensing and Digital Earth, CAS. Since 2017, he has been a Professor with Qingdao University, China. He has published more than 150 peer-reviewed papers, 30 international conferences papers, and six books. His research interests include remote sensing and geosciences, vegetation dynamics, statistical analysis, image processing, soil moisture and drought disaster, and air pollution remote sensing.

FENGMEI YAO received the Ph.D. degree in meteorology from the Institute of Atmospheric Physics, Chinese Academy of Sciences (CAS), Beijing, China, in 2005.

Since August 2005, she has been an Assistant Professor with the Graduated University of Chinese Academy of Sciences. Since 2017, she has been a Full Professor with the College of Earth and Planetary Sciences, University of Chinese Academy of Sciences. She has been involved in climate change and effect on vegetation and agriculture, atmospheric environment, and disaster. She has published more than 100 peer-reviewed papers, 20 international conferences papers, and four books.

SHAHZAD ALI was born in Peshawar, Pakistan, in 1988. He received the B.Sc. and M.Phil. degrees in agronomy from the University of Agriculture, Peshawar, in 2011 and 2013, respectively, and the Ph.D. degree in agronomy from Northwest A&F University, Yangling, China, in 2018.

Since 2018, he held a postdoctoral position with the Remote Sensing Information and Digital Earth Center, College of Computer Science and Technology, Qingdao University, Qingdao, China. He has authored more than 30 peer-reviewed articles. His research interests include remote sensing, GIS, agronomy, climate change, and irrigation agriculture.